Dispersion of Polystyrene Inside Polystyrene-*b*-poly(*N*-isopropylacrylamide) Micelles in Water

XIAODONG YE, JINGYI FEI, JUAN GUAN, XUECHANG ZHOU, GUANGZHAO ZHANG

Hefei National Laboratory for Physical Sciences at the Microscale, Department of Chemical Physics, University of Science and Technology of China, Hefei, Anhui 230026, China

Received 25 September 2009; revised 28 December 2009; accepted 29 December 2009
DOI: 10.1002/polb.21948
Published online in Wiley InterScience (www.interscience.wiley.com).

ABSTRACT: The addition of mixture of polystyrene-*b*-poly(*N*-isopropylacrylamide) (PS-*b*-PNIPAM) and polystyrene homopolymer (*h*-PS) in tetrahydrofuran dropwise into water leads to nanoparticles with a PS core and a thermally sensitive PNIPAM shell. The effects of the ratio of the homopolymer to copolymer and temperature on the formation and stabilization of the dispersion were investigated by using a combination of static and dynamic laser light scattering. PNIPAM shell continuously collapses as temperature increases in the range 20–40 °C. Such formed particles are stable even at temperatures much higher than lower critical solution temperature (LCST ~ 32 °C) of PNIPAM. Our results reveal that the area occupied *per* hydrophilic PNIPAM chain on the hydrophobic PS core remains nearly a constant regardless of the amount of *h*-PS in the polymer mixture. This clearly indicates that the surface area occupied *per* hydrophilic group is a critical parameter for stabilizing particles dispersed in water. © 2010 Wiley Periodicals, Inc. J Polym Sci Part B: Polym Phys 48: 749–755, 2010

KEYWORDS: diblock copolymers; dispersions; light scattering; micelles; poly(ethylene oxide); poly(*N*-isopropylacrylamide); polystyrene; stabilization; stimuli-sensitive polymers

INTRODUCTION As an old issue, colloidal stabilization relates to phase behavior, structure, and properties of particulate suspensions. It is important in pharmacy, ceramics, paints, pigments, and other industries today. Because of the large attractive van der Waals' interactions, colloids usually irreversibly aggregate. Generally, to stabilize colloidal dispersions, charged groups or short polymer chains are introduced to colloid surface, so that the interactions between the attractive van der Waals' forces can be balanced by Coulombic or other steric-repulsive interactions.[1,2] Recently, a so-called nanoparticle haloing strategy was introduced where colloids were stabilized by highly charged small nanoparticles.[3] Such nanoparticles induce effective repulsion. Considering that the small nanoparticles, charged groups, polymer chains, and surfactants are stabilizers of colloids, quantitatively understanding the role of a stabilizer is important for controlling the colloidal stabilization. On the basis of the assumption that the hydrophobic tail of the stabilizer is on the surface of the particles, which is an idealized micelle structure, Antonietti et al.[4,5] proposed a model, where the particle radius can be calculated with the weight ratio of emulsifier to polymer. Using a more simple model, Wu predicted that for a given dispersion, the particle surface area occupied per stabilizer is a constant.[6] Such a model has been tested valid in several polymeric colloid systems.[7,8]

Besides small nanoparticles, charged groups, polymer chains, and surfactants, block copolymers can also be used as stabilizers. When a copolymer is dissolved in a solvent which is a nonsolvent for one block and a good solvent for the other, the copolymer may form micelles in solution. The micelles have the ability to solubilize homopolymer in solution and form stable dispersions, which have been studied both theoretically[9–11] and experimentally.[12–16] Theoretically, Viduna et al. studied the conformation of solubilized homopolymer chains and core-forming blocks by Monte Carlo Simulation.[9] Izzo and Marques found that the maximum amount of solubilized homopolymer in 1 g of copolymer decreases with the polymerization index of the homopolymer.[10] Experimentally, Tuzar et al. investigated the solubilization of two polybutadiene homopolymers and a triblock copolymer polystyrene-*b*-polybutadiene-*b*-polystyrene micelles with a high content of butadiene in the polybutadiene cores of polystyrene-*b*-polybutadiene-*b*-polystyrene micelles by light scattering.[12] They found that the maximum amount of solubilized polybutadiene based on the weight of the copolymer was 60 wt %. Using laser light scattering, Quintana et al. studied the solubilization of polyisobutylene by micelles of polystyrene-*b*-poly(ethylene/propylene) block copolymer in several selective solvents and found that the maximum of solubilized polyisobutylene decreases with the polymerization index of the polyisobutylene homopolymer.[13,14] Besides the systems in organic solvents, aqueous systems have also been studied. Eisenberg et al. studied the formation of crew-cut aggregates from blends of polystyrene-*b*-poly(acrylic acid) diblock copolymer and polystyrene homopolymer in aqueous solution

Correspondence to: X. Ye (E-mail: xdye@ustc.edu.cn)
Journal of Polymer Science: Part B: Polymer Physics, Vol. 48, 749–755 (2010)

by static light scattering and transmission electron microscopy.[15] Liu et al. reported a novel and simple approach to prepare micelles and hollow spheres through self-assembly of poly(ε-caprolactone) homopolymer and a random copolymer with short poly(ε-caprolactone) as side chains.[16]

On the other hand, the synthesis and self-assembly of block copolymers with one thermosensitive block and one hydrophobic block have been reported. Among the thermosensitive polymers studied, poly(*N*-isopropylacrylamide) (PNIPAM) with a lower critical solution temperature (LCST) at ~32 °C has been extensively used.[17–19] Cho et al. have synthesized diblock copolymer consisting of PNIPAM as hydrophilic block and poly(γ-benzyl L-glutamate) as hydrophobic block.[20,21] The core-shell nanoparticles were obtained by the diafiltration method. The size of the nanoparticles was unchanged between 25 and 40 °C. While it was found that the size distribution of the nanoparticles was very large. Tenhu et al. have investigated the micellization behavior of series of amphiphilic diblock copolymers comprising PNIPAM as a thermosensitive block with hydrophobic blocks, either polystyrene or poly(*tert*-butyl methacrylate).[22] Micellar particles were formed when the length of the PNIPAM block was shorter and it was unexpected that the micellar particles were stable even at the temperature above LCST of PNIPAM. Recently, Hamley and coworkers have prepared poly(methyl methyacrylate)-*b*-poly(*N*-isopropylacrylamide) amphiphilic block copolymers and studied the formation and stability of the micelles.[23] They found that the micelles aggregated when the temperature was above LCST of PNIPAM. So far, solubilization of homopolymer by using these kinds of amphiphilic block copolymers with one thermosensitive block has received less attention.

In the present work, we have prepared polymeric colloids consisting of polystyrene-*b*-poly(*N*-isopropylacrylamide) (PS-*b*-PNIPAM) and polystyrene homopolymer (*h*-PS) in water, where PS blocks and *h*-PS are expected to form the core and PNIPAM blocks form the shell. The increase of the amount of *h*-PS leads to the increase in the size of the hydrophobic PS core, while the area stabilized by per hydrophilic PNIPAM is close to a constant. By using of a combination of static and dynamic laser light scattering, we have investigated the stabilization of the colloidal particles. Our objective is to understand the relation between the surface area per stabilizer and the stabilization of the dispersion in aqueous solution.

EXPERIMENTAL

Sample Preparation

Styrene was first washed three times with NaOH aqueous solution and then with water to remove the resultant salts and residual NaOH. Finally, styrene was distilled under reduced pressure over calcium hydride. *N*-isopropylacrylamide (NIPAM, Aldrich) was purified by recrystallization from a mixture of benzene and *n*-hexane. 4,4′-Azobis(isobutyronitrile) (AIBN; Fluka, 98%) were purified by recrystallization from ethanol. Tetrahydrofuran (THF) was distilled from a purple sodium ketyl solution. The details about the synthesis and characterization of PS-*b*-PNIPAM diblock copolymer can be found elsewhere.[24–26] Molecular weight and molecular weight distribution (M_w/M_n) were determined by gel permeation chromatography (GPC) on a Waters 150C by use of monodisperse polystyrene as the calibration standard and THF as the eluent with a flow rate of 1.0 mL/min. PS-*b*-PNIPAM copolymer used contains 207 PS units and 357 PNIPAM units. The polydispersity index (M_w/M_n) is 1.17. Polystyrene homopolymer (*h*-PS, Shodex; $M_w = 1.36 \times 10^4$ g/mol, $M_w/M_n = 1.02$) contains 131 PS units.

Dispersion Preparation

The micellization of PS-*b*-PNIPAM with a certain amount of *h*-PS was induced by adding 0.4 mL solution of PS-*b*-PNIPAM and *h*-PS in THF dropwise into 40 mL of deionized water under stirring at 20 °C. Such prepared dispersions were stabilized by the hydrophilic PNIPAM shell. The initial PS-*b*-PNIPAM concentration in THF solution was kept as 3.3×10^{-4} g/mL. The small amount of THF (1 wt %) introduced in the preparation was removed by evaporation under reduced pressure.

Laser Light Scattering and Zeta Potential Measurements

A commercial LLS spectrometer (ALV/DLS/SLS-5022F) equipped with a multi-τ digital time correlator (ALV5000) and a cylindrical 22 mW UNIPHASE He–Ne laser ($\lambda_0 = 632.8$ nm) as the light source was used. In static LLS,[27,28] the angular dependence of the absolute excess time-average scattering intensity, known as the Rayleigh ratio $R_{vv}(q)$, was recorded, and we were able to obtain the weight-average molar mass (M_w), the root-mean-square radius of gyration $\langle R_g^2 \rangle_z^{1/2}$ (or written as $\langle R_g \rangle$), and the second virial coefficient A_2 by using

$$\frac{KC}{R_{vv}(q)} \approx \frac{1}{M_w}\left(1 + \frac{1}{3}\left\langle R_g^2 \right\rangle_z q^2\right) + 2A_2C \approx \frac{1}{M_w}\left(1 + \frac{1}{3}\left\langle R_g^2 \right\rangle_z q^2\right) \quad (1)$$

where $K = 4\pi^2(dn/dC)^2/(N_A\lambda_0^4)$ and $q = (4\pi n/\lambda_0)\sin(\theta/2)$ with C, dn/dC, N_A, and λ_0 being concentration of the polymer, the specific refractive index increment, the Avogadro's number, and the wavelength of light in a vacuum, respectively. The extrapolation of $R_{vv}(q)$ to $\theta \to 0$ and $C \to 0$ leads to M_w. In this study, the concentration in all the experiments is so low that extrapolation to infinite dilution was not necessary and the plot of $[KC/R_{vv}(q)]$ versus q^2 leads to $\langle R_g \rangle$. The specific refractive index increments of the polymeric aggregates were calculated using an addition method.[29] In dynamic LLS,[30] the Laplace inversion of a measured intensity-intensity time correlation function $G^{(2)}(t, q)$ in the self-beating mode results in a line-width distribution $G(\Gamma)$. For a pure diffusive relaxation, Γ is related to the translational diffusion coefficient D by $\Gamma/q^2 = D$, which is further related to the hydrodynamic radius $R_h = k_BT/(6\pi\eta D)$ with k_B, T, and η being the Boltzman constant, the absolute temperature, and the solvent viscosity, respectively. Zeta potential measurements of core-shell nanoparticles were carried out on a Malvern Zetasizer Nano ZS90 instruments with a He–Ne Laser and 90° collecting optics.

RESULTS AND DISCUSSION

Figure 1 shows that the average hydrodynamic radius $\langle R_h \rangle$ and average radius of gyration $\langle R_g \rangle$ of the dispersion as a function of the *h*-PS weight fraction (f_{PS}) which is defined as the ratio of the weight of *h*-PS ($W_{h\text{-PS}}$) to the total weight of *h*-PS and PS-*b*-PNIPAM ($W_{h\text{-PS}} + W_{\text{PS-}b\text{-PNIPAM}}$) at 25 °C. Our preliminary experiments demonstrated that PS dispersion is stable when $f_{PS} < \sim 33$ wt %. The introduction of more *h*-PS leads to macroscopic precipitation. This is because the hydrophilic PNIPAM blocks can only stabilize a certain surface area of the particles. Similarly, Tuzar et al. shows that the maximum amount of solubilized polybutadiene by a three-block copolymer poly(styrene–butadiene–styrene) was 60 wt % based on the weight of the copolymer,[12] which means that the weight fraction based on the total weight of homopolymer and block copolymer was ~38 wt %. When the amount of polybutadiene homopolymer was higher than 38 wt %, the solution was unstable. Note that the zeta potential of the core-shell nanoparticles was slightly negative between −6 and −3 mV, which is consistent with the value of PNIPAM grafted P(PNIPAM-*co*-styrene) core-shell nanoparticle (−3.5 mV),[31] indicating that the electrostatic interaction may contribute to some extent to the stability of the dispersion here. In comparison with the micelles formed only by PS-*b*-PNIPAM block copolymers, the addition of *h*-PS lead either $\langle R_h \rangle$ or $\langle R_g \rangle$ to increase slightly, suggesting an increase in the micellar dimensions and indicating that more *h*-PS have been accumulated and stabilized by PS-*b*-PNIPAM in each core-shell particle.

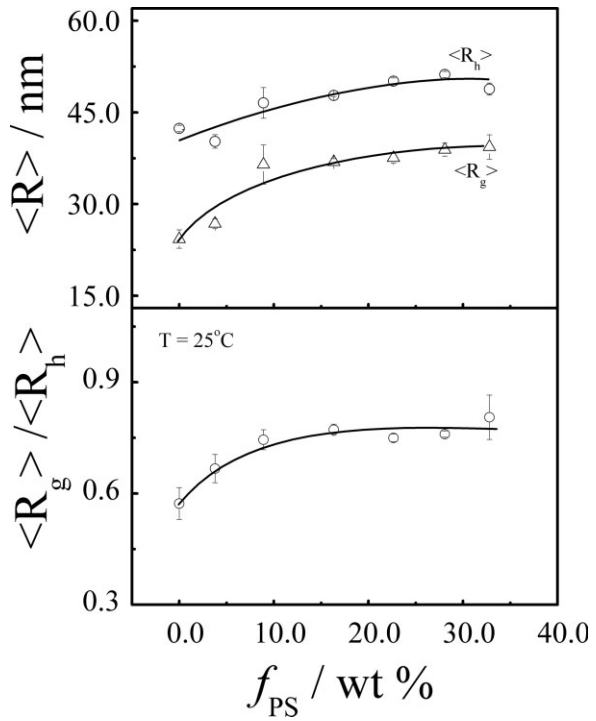

FIGURE 1 h-PS content (f_{PS}) dependence of average hydrodynamic radius $\langle R_h \rangle$, average radius of gyration $\langle R_g \rangle$ and their ratio $\langle R_g \rangle / \langle R_h \rangle$ of core-shell particles (*h*-PS dispersion), where f_{PS} is defined as $f_{PS} = W_{h\text{-PS}}/(W_{h\text{-PS}} + W_{\text{PS-}b\text{-PNIPAM}})$.

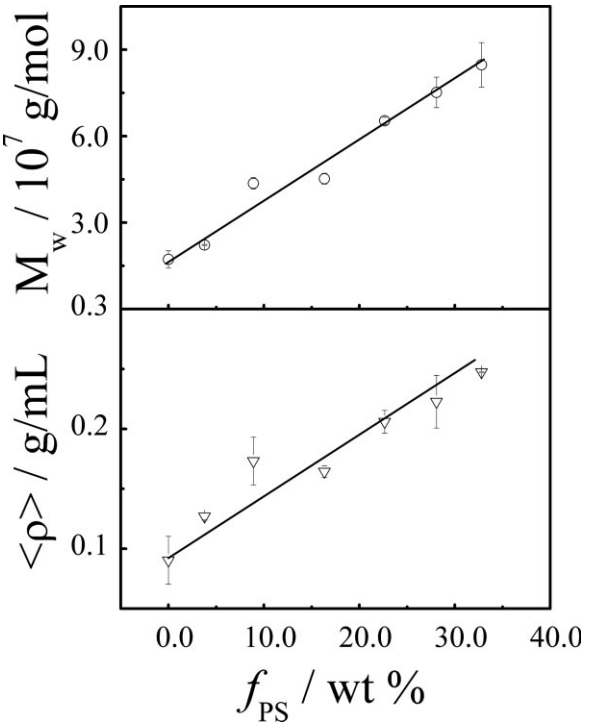

FIGURE 2 Plots of the apparent molecular weight (M_w) and the average density of the micelles versus f_{PS}, where $\langle \rho \rangle$ is defined as $\langle \rho \rangle = M_w / \left(\frac{4}{3}\pi \langle R_h \rangle^3 N_A\right)$.

The structure of the particles can be better viewed in terms of $\langle R_g \rangle / \langle R_h \rangle$. It is known that for a uniform and nondraining sphere, $\langle R_g \rangle / \langle R_h \rangle = 0.78$; for a linear flexible random chain in a good solvent, $\langle R_g \rangle / \langle R_h \rangle = 1.5$.[32] As f_{PS} increases from 0 to 8.9 wt %, $\langle R_g \rangle / \langle R_h \rangle$ increases from 0.58 to 0.75. This is because the collapsed and dense PS core becomes larger, and the effect of the swollen PNIPAM shell on $\langle R_g \rangle$ and $\langle R_h \rangle$ decreases so that the particles become more uniform. Further increasing f_{PS} from 8.9 to 32.8 wt % no longer varies $\langle R_g \rangle / \langle R_h \rangle$ because the particles tend to be uniform and nondraining. Namely, the addition of *h*-PS leads both $\langle R_g \rangle$ and $\langle R_h \rangle$ to increase but their ratio $\langle R_g \rangle / \langle R_h \rangle$ almost holds. Figure 2 shows that the apparent weight average molar mass (M_w) and the average density ($\langle \rho \rangle$) of the dispersion increase with f_{PS}, further indicating that the core of the micelles becomes denser. Note that even the maximum density (~0.25 g/mL) is still much lower than that of bulk PS or bulk PNIPAM (~1 g/mL). This is because that the PS chains in the core are unsolvated, i.e., the density of the PS core is close to that of the bulk PS (~1 g/mL), while the PNIPAM chains in the corona are highly solvated, which means that the density of the PNIPAM corona is much less than that of the bulk PNIPAM. Wu has reported that the densities of the PNIPAM microgel and PNIPAM linear chains in water at 30.0 °C are 0.021 and 0.0063 g/mL,[33] respectively, which are smaller than the density of the core-shell nanoparticles due to the existence of the unsolvated PS core here.

Because *h*-PS and PS-*b*-PNIPAM polymer chains were mixed homogenously in THF solution, we can assume that the

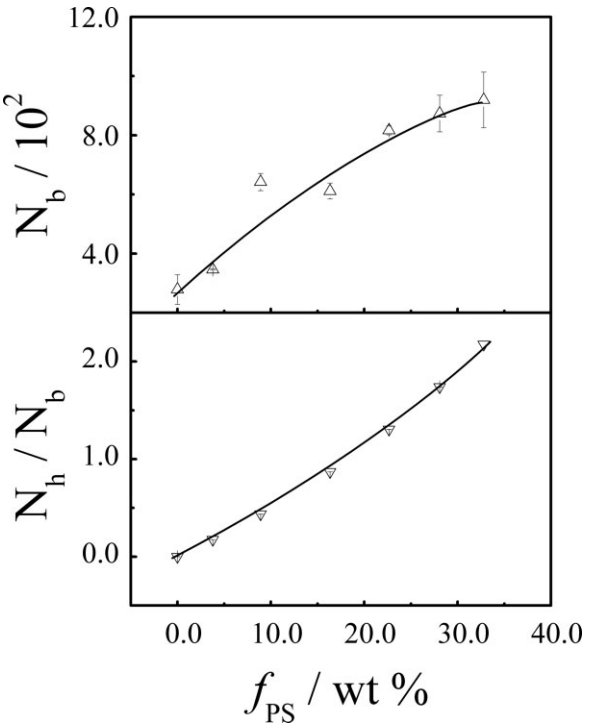

FIGURE 3 Plots of the number of PS-*b*-PNIPAM (N_b) and the ratio of N_h to N_b in each core-shell particle versus f_{PS}.

composition of each micelle in aqueous solution is equal to that in original THF solution. From the composition of the micelles, M_w of the nanoparticles, PS-*b*-PNIPAM diblock copolymer ($M_{PS\text{-}b\text{-}PNIPAM}$) and PS homopolymer ($M_{PS}$), we were able to calculate the average number of diblock copolymer (N_b) and PS homopolymer (N_h) inside each nanoparticle by using eqs 2 and 3,

$$N_b = [M_w \times (1 - f_{PS})/M_{PS\text{-b-PNIPAM}}] \quad (2)$$

$$N_h = [M_w \times f_{PS}/M_{PS}] \quad (3)$$

Figure 3 shows that both N_b and the ratio N_h/N_b increase with f_{PS}. As more *h*-PS was trapped in the micelle, N_h increases. Because of the increase in N_h, to stabilize the dispersion N_b also increase but for a small magnitude because the PS-*b*-PNIPAM is supposed to stabilize the surface of the dispersion. This is the reason that N_h/N_b increases with f_{PS}.

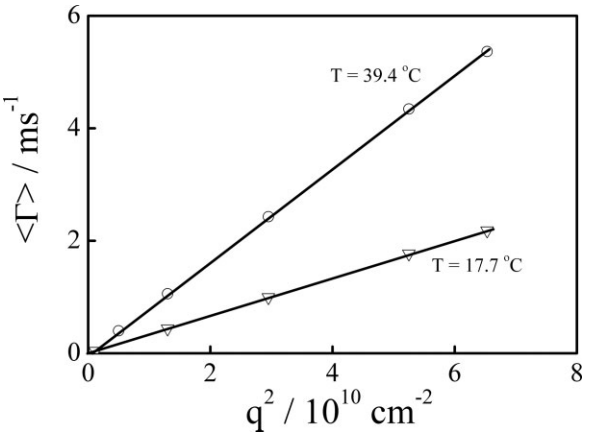

FIGURE 4 Scattering vector (***q***) dependence of the characteristic linewidth ($\langle\Gamma\rangle$) of the micelles, where f_{PS} was 8.9 wt %.

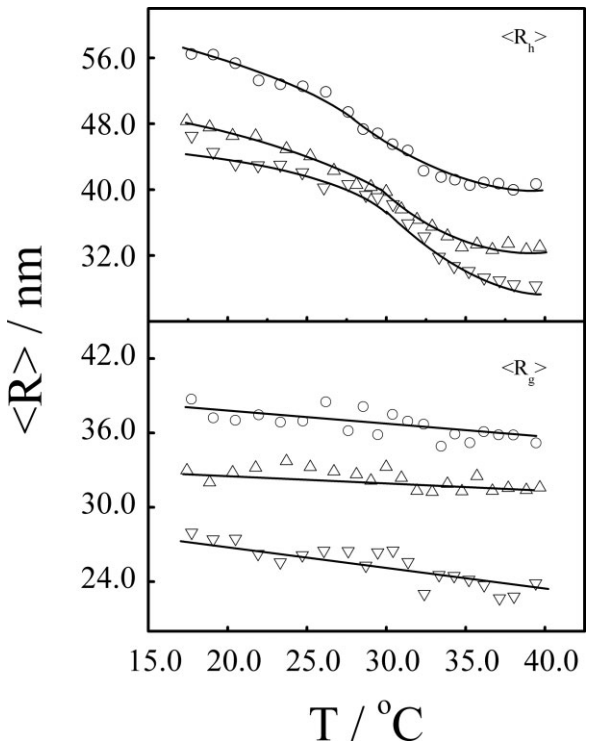

FIGURE 5 Temperature dependence of average hydrodynamic radius $\langle R_h\rangle$ and average radius of gyration $\langle R_g\rangle$, where f_{PS} were 0 wt % (▽), 8.9 wt % (Δ), and 32.8 wt % (O), respectively. Relative errors: $\langle R_g\rangle$: ±8%; $\langle R_h\rangle$: ±2%.

Figure 4 shows that the scattering vector (***q***) dependence of the average line width $\langle\Gamma\rangle$. The linear $\langle\Gamma\rangle$ versus $\boldsymbol{q}^2$ relation at different temperatures indicates that the micelles have an isotropic diffusive behavior. Figure 5 shows that as the temperature increases, $\langle R_h\rangle$ gradually decreases, while $\langle R_g\rangle$ slightly decreases, i.e., the micelles undergo a continuous collapse transition. Such a continuous collapse transition has been observed for PNIPAM chains attached on polystyrene latex[34,35] and planar gold surface.[36–38] The nonuniformity of the chains as well as the surface constraint were thought to be responsible for the continuity.[39–42] It is worth noting that crosslinked PNIPAM gels[43,44] and individual PNIPAM chains with narrowly distributed high molar mass[19] show a sharp volume change at ~33 °C. Note that double phase transition of PNIPAM chains has been reported by Tenhu et al. and Liu et al. Tenhu et al. prepared gold nanoparticles stabilized with two types of PNIPAMs via the "grafting to" approach and found the PNIPAM brushes with a grafting density of 0.42 nm^2/chain exhibit two separate phase transitions.[25] The PNIPAM segments in the inner zone undergo the first transition at lower temperature and PNIPAM segments in the outer zone show the second transition at higher temperature. Liu et al. synthesized silica nanoparticles grafted with

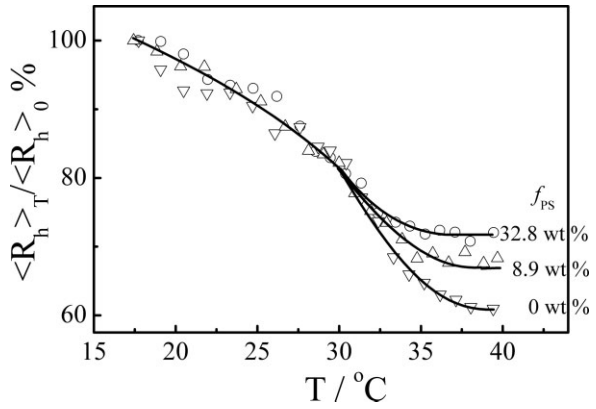

FIGURE 6 Temperature dependence of $\langle R_h \rangle_T / \langle R_h \rangle_0$ during the heating process, where $\langle R_h \rangle_T$ and $\langle R_h \rangle_0$ are the average hydrodynamic radius of core-shell particles at the temperature T and 17.5 °C.

PNIPAM brushes with a grafting density of ~2 nm^2/chain and also found double thermal phase transition.[45] We did not observe double phase transition maybe because of the relatively lower grafting density of PNIPAM chains in our experiments, which we will discuss later. It should be stated that there is no plateau at the temperature around 20 °C. This phenomenon has also been observed in the study of phase transition by laser light scattering[45,46] and QCM,[38] which may be explained as at this temperature the PNIPAM random coils or chains on the surface are still not fully hydrated and extended. Figure 5 also shows that $\langle R_g \rangle$ of the PS dispersion stabilized with PS-*b*-PNIPAM decreases more slowly than that of PS-*b*-PNIPAM micelles. This is because the increase of PS weight in the dispersion makes the weight of PS dominant and the effect of the shrinking of PNIPAM play less importance on the decrease of $\langle R_g \rangle$. This influence is much more obvious for the decrease of $\langle R_g \rangle$ than that of $\langle R_h \rangle$. To show clearly the effect of the temperature on the $\langle R_h \rangle$, the data in Figure 5 have been replotted in Figure 6 in terms of percentage change in hydrodynamic radius. Figure 6 shows the temperature dependence of $\langle R_h \rangle_T / \langle R_h \rangle_0$, where $\langle R_h \rangle_T$ and $\langle R_h \rangle_0$ are the average hydrodynamic radius of core-shell particles at the temperature T and 17.5 °C. Presumably, the PS core is unaffected by the change in temperature, the change in $\langle R_h \rangle$ is because of the dehydration of the PNIPAM corona. $\langle R_h \rangle_T / \langle R_h \rangle_0$ increases from 61 to 72% with the increase in f_{PS} from 0% to 32.8 wt %, which also indicates that the PNIPAM corona has less effect on hydrodynamic radius when f_{PS} increases.

Our experimental results also show that the weight average molar masses of the micelles slightly change as the temperature increases, i.e., no aggregation occurs when PNIPAM corona collapses. In other words, the micelles are stable even at a temperature much higher than the LCST of PNIPAM. Such a phenomenon has been observed before.[22,47] The stabilization of the dispersion can be explained in terms of viscoelasticity. The aggregation of the micelles is controlled by the average time of the collisions. Only when the collision time (τ_c) is longer than the time (τ_e) for a permanent chain overlapping entanglement between two approaching micelles, can they come into fusion.[48,49] As PNIPAM chains consisting of the micelle corona are short, even at the temperatures below the LCST of PNIPAM, the tethered chains have much smaller contact area than the free chains. In other word, $\tau_e > \tau_c$, so that they have less chances to stick together. Meanwhile, the surface constraint prevents the grafted chains from complete dehydrating, further stabilizing the micelles. Note that Tang et al. shows that core-shell nanoparticles of poly(methyl methacrylate)-*b*-poly(*N*-isopropylacrylamide) diblock copolymers aggregate at ~32 °C, which maybe due to the relatively higher concentration (0.5 wt %) of the diblock copolymers compared with the concentrations ($<5 \times 10^{-6}$ g/mL) of the core-shell nanoparticles in our experiments.[23]

Assuming the average hydrodynamic radius $\langle R_h \rangle$ of the micelles at most collapsed state is equal to the average radius of the core of the micelle and the number of the PS-*b*-PNIPAM chains in the micelle can be obtained as shown in Figure 3, we can calculate that the surface area (s) occupied per PNIPAM chain is about 23 nm^2. However, the assumption that the hydrodynamic radius in the most collapsed state is equal to the average radius of the core of the micelle overestimate the size of the micelle core because we ignore the thickness of the collapsed PNIPAM corona. To obtain more accurate s, we have to estimate the thickness of the collapsed PNIPAM corona. By using a self-consistent field (SCF) developed by Milner et al., the height h of a brush is proportional to polymerization index.[50] In addition, It has been shown by Brooks et al. that the hydrodynamic thickness of the PNIPAM brush (M_n = 796,000, M_w/M_n = 1.26) at the most collapsed state is ~100 nm.[35] Note that the grafting density of their PNIPAM brush is 23 nm^2, which is similar to that of the PNIPAM brush here. The molecular weight of PNIPAM block is 4×10^4 g/mol. Therefore, the thickness of the PNIPAM brush at the most collapsed state can be estimated as ~5 nm. Then the s values can be recalculated and the data have been shown in Figure 7. From Figure 7 we know s is about 19 nm^2, which is independent of f_{PS}, i.e., for the micelles with or without the solubilized *h*-PS, each PNIPAM

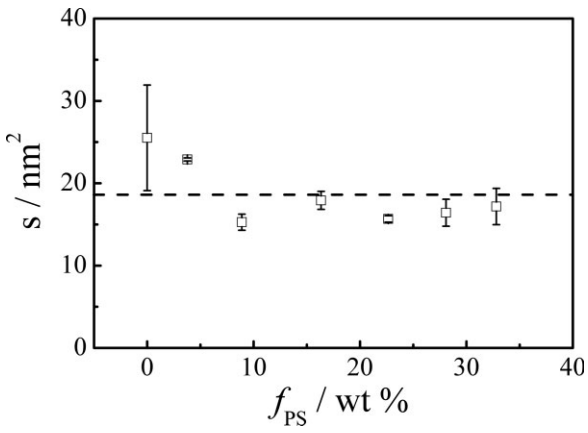

FIGURE 7 A plot of the average surface area (s) occupied by each diblock copolymer PS-*b*-PNIPAM versus f_{PS}.

occupy a certain area. Such relation has been tested valid in polymeric nanoparticles stabilized by surfactant, ionic groups, and polymer chains. The present study further indicate such a relation is general for a stable polymeric particles manipulated by hydrophobic–hydrophilic interaction balance. Note that the value *s* is higher than those reported by Tenhu et al.[25] and Liu et al.,[45] which maybe the reason we did not observe double phase transition.

CONCLUSIONS

Polystyrene dispersion can be stabilized by amphiphilic diblock copolymer PS-*b*-PNIPAM. The light scattering studies on the amount of hydrophobic *h*-PS as a function of temperature demonstrate that the particles are stable even at temperatures higher than LCST of PNIPAM. As temperature increases, PNIPAM shell continuously collapses in the temperature range 20–40 °C. The area occupied per hydrophilic PNIPAM chain on the hydrophobic PS core holds a constant independent of the amount of *h*-PS, and hence it is a critical parameter for stabilization of polymeric particles in water.

The financial support of the National Natural Scientific Foundation of China (NNSFC) Projects (20804043) and Specialized Research Fund for the Doctoral Program of Higher Education (200803581022) is gratefully acknowledged.

REFERENCES AND NOTES

1 Hunter, R. J. In Foundations of Colloid Science; Oxford University Press: Oxford, 2001.

2 Verwey, E. J. W.; Overbeek, J. Th. G. In Theory of the Stability of Lyophobic Colloids; Elsevier: Amsterdam, 1948.

3 Tohver, V.; Smay, J. E.; Braem, A.; Braun, P. V.; Lewis, J. A. Proc Natl Acad Sci USA 2001, 98, 8950–8954.

4 Antonietti, M.; Bremser, W.; Schmidt, M. Macromolecules 1990, 23, 3796–3805.

5 Antonietti, M.; Bremser, W.; Muschenborn, D.; Rosenauer, C.; Schupp, B.; Schmidt, M. Macromolecules 1991, 24, 6636–6643.

6 Wu, C. Macromolecules 1994, 27, 298–299.

7 Wu, C. Macromolecules 1994, 27, 7099–7102.

8 Wu, C.; Akashi, M.; Chen, M. Q. Macromolecules 1997, 30, 2187–2189.

9 Viduna, D.; Limpouchova, Z.; Prochazka, K. Macromol Theory Simul 2001, 10, 165–173.

10 Izzo, D.; Marques, C. M. J Phys Chem B 2005, 109, 6140–6145.

11 Lefebvre, M. D.; Shull, K. R. Macromolecules 2006, 39, 3450–3457.

12 Tuzar, Z.; Bahadur, P.; Kratochivíl, P. Makromol Chem 1981, 182, 1751–1760.

13 Quintana, J. R.; Salazar, R. A.; Katime, I. Macromolecules 1994, 27, 665–668.

14 Quintana, J. R.; Salazar, R.; Katime, I. J Phys Chem 1995, 99, 3723–3731.

15 Zhang, L.; Eisenberg, A. J Polym Sci Part B: Polym Phys 1999, 37, 1469–1484.

16 Liu, X. Y.; Jiang, M.; Yang, S. L.; Chen, M. Q.; Chen, D. Y.; Yang, C.; Wu, K. Angew Chem Int Ed Engl 2002, 41, 2950–2953.

17 Schild, H. G. Prog Polym Sci 1992, 17, 163–249.

18 Winnik, F. M. Macromolecules 1990, 23, 233–242.

19 Wu, C.; Zhou, S. Q. Macromolecules 1995, 28, 8381–8387.

20 Cho, C. S.; Cheon, J. B.; Jeong, Y. I.; Kim, I. S.; Kim, S. H.; Akaike, T. Macromol Rapid Commun 1997, 18, 361–369.

21 Cho, C. S. Polymer 1999, 40, 2041–2050.

22 Nuopponen, M.; Ojala, J.; Tenhu, H. Polymer 2004, 45, 3643–3650.

23 Tang, T.; Castelleto, V.; Parras, P.; Hamley, I. W.; King, S. M.; Roy, D.; Perrier, S.; Hoogenboom, R.; Schubert, U. S. Macromol Chem Phys 2006, 207, 1718–1726.

24 Zhang, W. A.; Zhou, X. C.; Li, H.; Fang, Y. E.; Zhang, G. Z. Macromolecules 2005, 38, 909–914.

25 Shan, J.; Chen, J.; Nuopponen, M.; Tenhu, H. Langmuir 2004, 20, 4671–4676.

26 (a) Thang, S. H.; Chong, Y. K.; Mayadunne, R. T. A.; Moad, G.; Rizzardo, E. Tetrahedron Lett 1999, 40, 2435–2438; (b) Goto, A.; Sato, K.; Tsujii, Y.; Fukuda, T.; Moad, G.; Rizzardo, E.; Thang, S. H. Macromolecules 2001, 34, 402–408.

27 Zimm, B. H. J Chem Phys 1948, 16, 1093–1099.

28 Chu, B. In Laser Light Scattering, 2nd ed.; Academic Press: New York, 1991.

29 Xia, J.; Dubin, P. In Macromolecular Complexes in Chemistry and Biology; Dubin, P.; Bock, J.; Davies, R. M.; Schultz, D. N.; Thies, C., Eds.; Spring-Verlag: New York, 1994; p 247.

30 Berne, B.; Pecora, R. In Dynamic Light Scattering; Plenum Press: New York, 1976.

31 Yin, W. Q.; Chen, M. Q.; Lu, T. H.; Akashi, M.; Huang, X. H. Eur Polym J 2006, 42, 2523–2531.

32 Burchard, W. In Light Scattering. Principles and Development; Brown, W., Ed.; Oxford University Press: Oxford, UK, 1996; pp 439–476.

33 Wu, C. Polymer 1998, 39, 4609–4619.

34 Zhu, P. W.; Napper, D. H. J Colloid Interface Sci 1994, 168, 380–385.

35 Kizhakkedathu, J. N.; Norris-Jones, R.; Brooks, D. E. Macromolecules 2004, 37, 734–743.

36 Balamurugan, S.; Mendez, S.; Balamurugan, S. S.; O'Brien, M. J.; Lopez, G. P. Langmuir 2003, 19, 2545–2549.

37 Zhang, G. Z. Macromolecules 2004, 37, 6553–6557.

38 Liu, G. M.; Zhang, G. Z. J Phys Chem B 2005, 109, 743–747.

39 Alexander, S. J Phys (Paris) 1977, 38, 983–987.

40 de Gennes, P. G. Macromolecules 1980, 13, 1069–1075.

41 Halperin, A.; Tirrell, M.; Lodge, T. P. Adv Polym Sci 1992, 100, 31–71.

42 Zhulina, E. B.; Borisov, O. V.; Pryamitsyn, V. A.; Birshtein, T. M. Macromolecules 1991, 24, 140–149.

43 Tanaka, T.; Sato, E.; Hirokawa, Y.; Hirotsu, S.; Peetermans, J. Phys Rev Lett 1985, 55, 2455–2458.

44 Hirose, Y.; Hirokawa, Y.; Tanaka, T. Macromolecules 1987, 20, 1342–1344.

45 Wu, T.; Zhang, Y. F.; Wang, X. F.; Liu, S. Y. Chem Mater 2008, 20, 101–109.

46 Wu, C.; Zhou, S. Q. Phys Rev Lett 1996, 77, 3053–3055.

47 Zhou, X. C.; Ye, X. D.; Zhang, G. Z. J Phys Chem B 2007, 111, 5111–5115.

48 Picarra, S.; Martinho, J. M. G. Macromolecules 2001, 34, 53–58.

49 Wu, C.; Li, W.; Zhu, X. X. Macromolecules 2004, 37, 4989–4992.

50 Milner, S. T.; Witten, T. A.; Cates, M. E. Macromolecules 1988, 21, 2610–2619.